Geophysical Research Letters

RESEARCH LETTER
10.1029/2019GL083988

Key Points:
- Twenty-five years of rawinsonde-based boundary layer depth was investigated at sites downwind of the Rocky and Appalachian Mountains.
- Large differences were present in boundary-layer depths due to the impact of elevated mixed layers advected off the mountains.
- The footprint of boundary layer depths over the plains is influenced by contrasting flows that change seasonally and spatially.

Supporting Information:
- Supporting Information S1

Correspondence to:
S. Pal,
sandip.pal@ttu.edu

Citation:
Pal, S., & Lee, T. R. (2019). Advected air mass reservoirs in the downwind of mountains and their roles in overrunning boundary layer depths over the plains. *Geophysical Research Letters*, *46*, 10,140–10,149. https://doi.org/10.1029/2019GL083988

Received 3 JUN 2019
Accepted 9 AUG 2019
Accepted article online 15 AUG 2019
Published online 26 AUG 2019

Advected Air Mass Reservoirs in the Downwind of Mountains and Their Roles in Overrunning Boundary Layer Depths Over the Plains

Sandip Pal[1] **and Temple R. Lee**[2,3]

[1]Department of Geosciences, Atmospheric Science Division, Texas Tech University, Lubbock, TX, USA, [2]Cooperative Institute for Mesoscale Meteorological Studies (CIMMS), Norman, OK, USA, [3]NOAA Air Resources Laboratory Atmospheric Turbulence and Diffusion Division, Oak Ridge, TN, USA

Abstract Atmospheric boundary layer depths (BLDs) over continental sites have long been meticulously characterized. However, a downwind-footprint concept for BLDs over plains under the impact of seasonally and spatially changing horizontal advection of BLDs off elevated terrains has remained unexplored. For the first time, we provide observational evidence of the impact of mountains on regional BLDs using 25-years (1991–2015) of rawinsonde-retrieved afternoon BLDs over 22 sites located in the mountains' (Rockies and Appalachians) downstream. Results suggest that mountain-advected air mass, elevated terrains, and wind play a significant role in modulating BLD variability "miles away" from terrains. We found significant BLD contrasts over the plains (400–1,500 m) under mountain-advected versus flatland-advected flows pertaining to elevated mixed layers off the mountain ranges. The BLD contrasts were higher in the downwind of Rockies than the Appalachians, and higher BLD contrasts were observed in spring and summer (900–1,500 m) than in fall and winter (100–500 m). These findings will help build advanced parameterizations in models where BLD simulations around complex terrain still remain a hurdle.

Plain Language Summary The study of Earth's atmospheric boundary layer is important for many applications, including improving weather and air quality forecasts. However, little is known about how the boundary layer behaves in the vicinity and "miles away" from mountains. In the present study, we investigated the variability in boundary layer depths in areas downwind of the Rocky Mountains and the Appalachian Mountains, using a novel technique recently developed to estimate the daytime maximum boundary layer depth from 25 years of observations derived from instrumented weather balloons. We found that boundary depths were much deeper when the wind was coming from the mountains, rather than from the nearby plains. Overall, our results underscore the importance of large-scale transport on certain characteristics of the atmospheric boundary layer, in particular temperature and moisture at sites downwind of large mountains. Knowledge gained from this study helps us improve how to better represent boundary layer processes in weather forecasting models and understand better thunderstorm development occurring over and near mountainous regions.

1. Introduction

The atmospheric boundary layer (ABL), a turbulent layer that couples the land surface and free troposphere, plays an important role in governing heat, mass, and momentum exchange (Stull, 1988); convection initiation (Groenemeijer et al., 2009) climate forcing (Davy & Esau, 2016) and aerosol cloud microphysics (Osborne et al., 2000). A key ABL parameter is the boundary layer depth (BLD; z_i) since it is one metric for defining the ABL. In the past, a number of studies investigated BLD spatial variability pertaining to underlying soil moisture heterogeneity (Reen et al., 2006) and topography (Kossmann et al., 1998). Other researchers attributed BLD spatial variability to coastal processes (Angevine et al., 2006), land use and land-cover changes (Pal et al., 2012), prevailing synoptic setup (Boutle et al., 2010), and meteorological conditions (Guo et al., 2019). However, it remains unclear how advection off the elevated terrains and associated large-scale transport of different air mass modulate ABL thermodynamics, in particular BLDs over the regions located in the mountains' downstream.

Analytical models treating the morphology of BLDs and energy exchange assume horizontally homogeneous conditions (e.g., Cai et al., 2014; Gryning & Batchvarova, 1999; Moeng & Rotunno, 1990).

Such numerical relationships are used in weather forecast and mesoscale simulations over locations (e.g., plains adjacent to mountains) where this assumption is not valid. One way to reduce the uncertainty due to parametrizations' restrictive assumptions is to increase model resolutions. Another way is to look into both the parametrizations and the aggregation methods (Koffi et al., 2016). Nevertheless, neither approaches considers the impact of the prevailing flow regimes and advection of ABL air mass reservoirs and their impact on regional-scale BLDs over the plains located in the mountains' downstream.

Meteorological processes over mountainous regions are complex, and there exists strong evidence that elevated terrains influence dynamical and convective processes over downstream regions (Fernando et al., 2015; Whiteman, 2000). Many past studies focused on the free troposphere and ABL flow regimes and associated thermodynamics (e.g., Rotach & Zardi, 2007), convection initiation (e.g., Behrendt et al., 2011), and tracer mixing (e.g., Fast et al., 2000) and less on the BLD variability, in particular over an extended regions in the mountains' downstream. For instance, the horizontal advection of elevated mixed layer (EML) frequently formed over terrains due to diurnal surface heating influences on convection initiation in the adjacent plains (e.g., Lanicci & Warner, 1991). Past studies mainly emphasized the formation and thermodynamic structures of EMLs over mountainous regions using aircraft measurements, rawinsonde observations, and numerical simulations (Demko et al., 2009; Stensrud, 1993); however, these studies did not report the impact of EMLs on BLD variability in the mountains' downstream. A few lidar-based studies provided evidence of enhanced BLDs in the adjacent plains where the authors speculated about downwind BLD enhancement (Nyeki et al., 2000; Pal et al., 2016). Understanding the role of advection-dominated atmospheric processes that control the BLDs over plains is important; for example, even model simulations with sufficient resolutions fail to resolve the impact of orography-induced flow modifications (Trentmann et al., 2009).

Impacts of mountain-induced flow modifications of BLDs have not yet been quantified systematically under varying meteorological conditions in the four seasons. It is important to assess how frequently and how far the EMLs impact BLDs over adjacent plains and an extended region "miles away" from mountains. Often, presence of EMLs yields meteorological conditions appropriate for deep moist convection (Lanicci & Warner, 1991). However, our knowledge remains limited about the impact of advected ABL air mass reservoirs in the downwind of mountains controlling ABL features.

Willis and Deardorff (1976) outlined that the horizontal advection of state variables can have as large an impact as turbulence in governing BLDs, even in presence of vigorous turbulence. However, direct evidence on the impact of horizontally advected EMLs overrunning the BLDs over adjacent plains remains unexplored. We hypothesize that under appropriate flow regimes, the impact of horizontal advection plays a decisive role in deepening the BLDs over the regions located mountains' downstream and can be quantified using the BLD measurements under two contrasting flow regimes: mountain downwind versus flatland downwind. We used 25 years (1991–2015) of rawinsonde observations over 22 sites in the contiguous United States located in the downwind of the Rocky and Appalachian Mountains (Figure 1) to (1) investigate the BLD contrasts under mountain-downwind versus flatland-downwind flow regimes, (2) understand how the impact of advected EMLs on the BLDs over mountains' downstream change during the four seasons, (3) determine how the BLD contrasts change spatially among the sites and regions, and (4) identify conditions when BLD contrasts might be linked to the impact of advected z_i off the elevated terrains on the plains.

2. Data Sets and Methods

Using an improved version of the bulk Richardson number (R_{ib}) approach (Lee & De Wekker, 2016; Lee & Pal, 2017), we computed the daily afternoon BLDs from the 00 UTC soundings available from the Integrated Global Radiosonde Archive (IGRA; Durre et al., 2006) for 22 sites (Figure 1). We determined the top of the ABL as the height at which the R_{ib} first exceeded 0.25 (e.g., Seidel et al., 2010, 2012; Vogelezang & Holtslag, 1996). The method used here reduces uncertainties related to shallow BLDs by removing near-surface stable layers (Lee & De Wekker, 2016; Pal & Lee, 2019).

The selected IGRA sites provide an ideal test bed to explore the "footprint" of BLDs over plains under mountain-advected flows because those sites span the entire Great Plains of the United States and lack significant coastal impact. Also, the formation of the EMLs is mainly controlled by the underlying topography (Lanicci & Warner, 1991); the selected IGRA sites are considered suitable for this study. We classified the

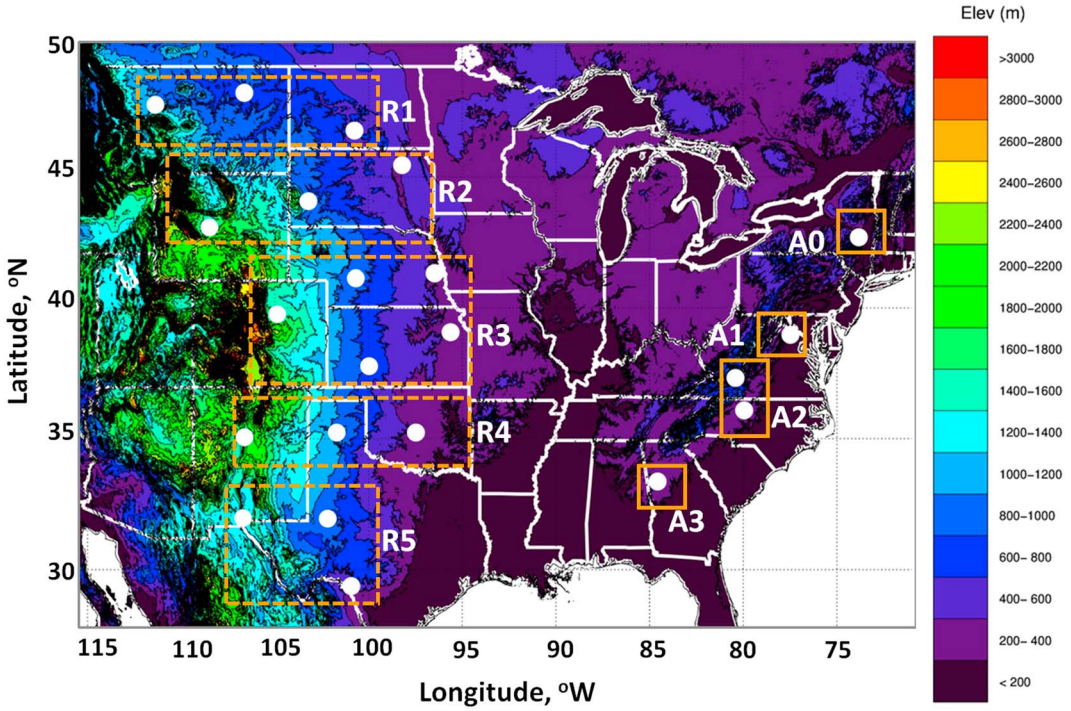

Figure 1. Locations of 22 Integrated Global Radiosonde Archive sites (white-filled circles) overlaid on the topographical maps (site elevation in m MSL) of six major regions (orange rectangles) in the contiguous United States located in the downwind of Rockies (R1, R2, R3, and R4), Mexican Plateau (R5), and Appalachians (A1–A5 sites). See Table S1 for additional details.

IGRA sites into two broad categories: R and A sites located in the downstream of Rocky and Appalachian Mountains, respectively. We further classified the R sites among five subcategories (R1, R2, R3, R4, and R5) and the A sites into four subcategories (A0, A1, A2, and A3) depending on the regions and latitudinal spans and broad geographical regions (Figure 1), as discussed in Lee and Pal (2017).

The number of profiles available varies among the sites (Table S1); however, except four sites (Santa Teresa, Albuquerque, Denver, and Riverton), all the sites have above 70% data coverage. Missing values in BLDs over all the sites occurred mainly due to unavailable measurements, and some erroneous soundings; they were not biased to any specific geographic location or year or season. After we estimated daily afternoon BLDs (henceforth, only BLDs) for individual profiles of the 25-year data sets, we determined the mean ABL wind direction (BL-WD) following Berman et al. (1999) and Pal and Lee (2019). The schematic (Figure 2a) illustrates the determination of BL-WD where we considered a 3-point running average of raw u and v wind components around $z_i/2$ from individual rawinsonde profiles and calculated mean wind direction at $z_i/2$.

We chose an arbitrary site Great Falls (a small city in northeast Montana, 1,130 m MSL), located in the downwind of west-southwesterly flow of the Rocky Mountains. Figure 2b shows wind-rose view of springtime daily BLD variability via frequency distribution analyses (BL-WD bin-width of 5°, thus 72 samples). We assigned mean mountain downwind flow to the BL-WD within a 60° angular sector (240–300°) with westerly (BL-WD of 270°) as a center. The closest mountain ridges (located ~100 km west of this site) vary between 1,800 and 2,300 m MSL. All the BLD samples obtained for the BL-WD of 240–300° (i.e., red arc sector in Figure 2b) were used to estimate the monthly median z_i under mountain downwind (z_i^{MD}). One should note that the angular sectors for other sites change according to the location of the sites with respect to the mountains but were always within a 60° arc. For z_i under flatland downwind (z_i^{FD}), we considered the opposite angular sector (i.e., 60–120°, blue arc sector) and estimated monthly median z_i^{FD}. Finally, to investigate the impact of advection of mountain-induced flows on the BLDs over a site located in downstream of terrains, we determined ΔBLD as

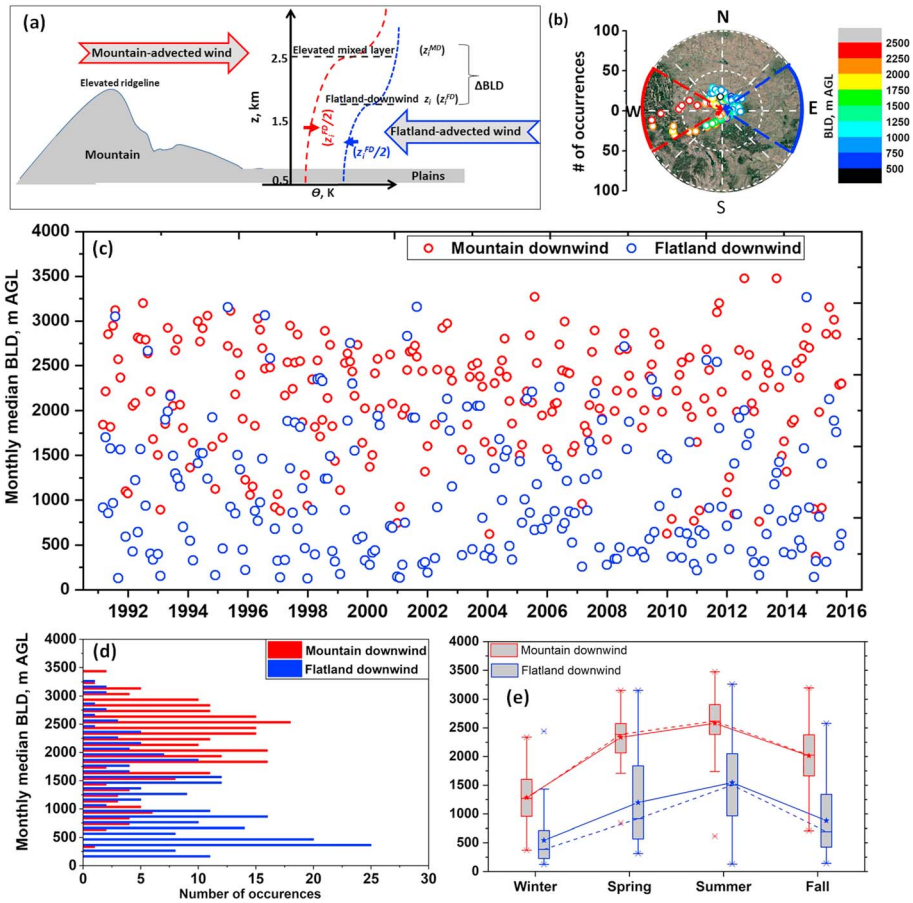

Figure 2. (a) Schematic illustrating BLD estimation under mountain-downwind (z_i^{MD}) versus flatland-downwind (z_i^{FD}) conditions where red and blue arrows mark advection from adjacent mountains and flatlands, respectively. Typical profiles of potential temperature (Θ) for both regimes are shown with the locations of elevated mixed layer top (red) and atmospheric boundary layer top (blue). (b) Wind-rose-type diagram yielding daily BLDs as a function of BL-WD via frequency distribution analysis (BL-WD bin width of 5° yielding 72 samples) for spring during the 25-year period at Great Falls, MT, overlaid on the satellite image of topography. Radii denote the number of occurrences, and angles mark the BL-WD. Red and blue dashed arrows with the arcs denote the 60° angular sectors selected for z_i^{MD} and z_i^{FD}, respectively. Colors mark the BLDs (m AGL). (c) Temporal variability in monthly median z_i^{MD} (red) and z_i^{FD} (blue) over Great Falls during the entire observation period (i.e., 300 samples for 25 years). (d) Frequency distributions of monthly median z_i^{MD} (red bars) and z_i^{FD} (blue bars) using a bin width of 100 m. (e) Overall climatological mean seasonal cycles of z_i^{MD} (red box and whiskers) and z_i^{FD} (blue) with solid and dashed lines connecting medians and means, respectively. BLD = boundary layer depth.

$$\Delta\mathrm{BLD} = z_i^{MD} - z_i^{FD}.$$

Over mountainous regions, thermodynamic structures during the late afternoon mostly favor quasi-stationary, well-mixed, terrain-independent spatial BLD variability (Pal et al., 2016) so that the BLD temporal variability on different time scales (e.g., day-to-day, seasonal, and intraseasonal) under two contrasting wind regimes (i.e., under mountain advection versus flatland advection) reflects the impact of terrains on BLDs over the flatland. Therefore, we estimated ΔBLDs to investigate the "footprint" of BLDs over plains under mountain-advected flows.

3. Results and Discussion

3.1. BLD Features Over the R1 Site Great Falls: An Example

A frequency distribution analysis of daily BLDs under various BL-WD regimes is presented in Figure 2b using a wind-rose-type diagram of all the retrieved BLDs over Great Falls in spring for the period 1991–2015

(see Supporting Information S1 for similar analyses for the other sites). Clearly visible is that BLDs under westerly flows (i.e., mountain downwind, z_i^{MD}) are higher than the BLDs under easterly flows (i.e., flatland downwind, z_i^{FD}). The temporal variability of monthly median z_i^{MD} and z_i^{FD} from 1991 to 2015 also confirm that except few cases z_i^{MD} is higher than z_i^{FD} (Figure 2c). To further quantify the impact of mountain-advected z_i on BLDs over the site, frequency distribution analyses of monthly median z_i^{MD} and z_i^{FD} for all four seasons over the entire measurement period (300 samples) were performed (Figure 2d; see Figure S2 for the other sites). The skewness for z_i^{MD} and z_i^{FD} distributions was −0.55 (left tailed) and 0.74 (right tailed), respectively. The histogram analyses confirmed that both mean and median of z_i^{MD} (2,148 and 2,220 m AGL, respectively) were higher than z_i^{FD} (1,112 and 890 m AGL, respectively), illustrating the impact of mountain-advected flows on the BLDs over the plains around Great Falls.

The box-and-whisker analyses of z_i^{MD} and z_i^{FD} for each season over the site (Figure 2e) show well-defined seasonal-scale patterns under both BL-WD regimes, which is typical BLD characteristic over land (Pal & Haeffelin, 2015). A striking feature is that z_i^{MD} is significantly higher than z_i^{FD} in all four seasons; ΔBLD was found to be at least 600 m throughout the year, which is substantial as soon as investigations related to skillful forecast of ABL features (Xie et al., 2013), convection initiation (Trier et al., 2004), and turbulence mixing of different tracers including air quality research (Lee et al., 2018) are considered. Additionally, while comparing the seasonal cycles of z_i^{MD} and z_i^{FD} with the overall seasonal cycle of median BLDs independent of flow regimes (i.e., without any BL-WD sampling), we found that the overall BLD seasonal cycle lies in between the two flow regimes: overall seasonal mean values were underestimated compared to z_i^{MD} and overestimated compared to z_i^{FD} (see Figure S3).

Figure 3 shows the daily BLD variability over Great Falls as a function of BL-WD via wind-rose-type diagrams (colored-filled contours) during the four seasons: winter, spring, summer, and fall (see Figure S1 for other sites for spring season). The color-bar scale limits vary among the panels to facilitate comparing BLDs under different BL-WD regimes not among seasons. Another note from the frequency distributions concerns the shape of the wind roses and how they change in each season affecting BLD variability, which illustrates that the key factor controlling the ΔBLDs during different seasons is the change in wind directionality. In general, deeper z_i^{MD} are found for westerly BL-WD regimes except summer when a secondary peak is also observed under southwesterly flows. The seasonal-scale variability is well explained by noting the distribution and spread of the EMLs as reflected in observed z_i^{MD} during the four seasons. Larger ΔBLD occurs in spring (~1,600 m) compared to the other seasons, most likely due to transport of drier air mass over the plains advected off the elevated terrains.

To further quantify the observed ΔBLD over Great Falls, a scatter diagram of all monthly median z_i^{MD} versus z_i^{FD} (i.e., 300 samples for 25 years) with a one-to-one line overlaid is presented in Figure 3e, which yields mostly higher ΔBLDs under the mountain-advected flow regime (see Figure S4 for other sites). Few cases (19 samples, 6% cases; Figure 3e) show that observed z_i^{MD} was less than z_i^{FD}; these cases most likely occurred because the meteorological conditions were not appropriate for the development of EMLs. Nevertheless, strikingly higher ΔBLDs (>1,500 m) were observed for the cases with $z_i^{MD} > 2{,}500$ m AGL pertaining to the influence of EMLs. Lanicci and Warner (1991) reported that dry-adiabatic EMLs over potentially moist layer often dominates this region, particularly in spring.

3.2. BLD Seasonal Cycles Over 22 IGRA Sites

To explore how horizontal advection plays an important role in deepening the BLDs locally, we investigated the climatological-averaged seasonal-cycle patterns of median BLDs for all the sites using Hovmöller-type diagrams of z_i^{MD} (Figure 4a) and z_i^{FD} (Figure 4b). The primary objective for analyzing overall seasonal-cycle patterns of z_i^{MD} and z_i^{FD} was to determine site-specific characteristics and spatial variability of the EMLs' impact on BLDs over adjacent flatland and immediate surrounding regions during each season in a composite mode, rather than being limited to a few case studies. These results reveal the impact of advected z_i off the regions of elevated terrains on BLDs over flat terrains located in the mountains' downstream, as can be clearly seen that in general z_i^{MD} is deeper (warmer color) than z_i^{FD} in all seasons (cooler color), in particular in spring and summer.

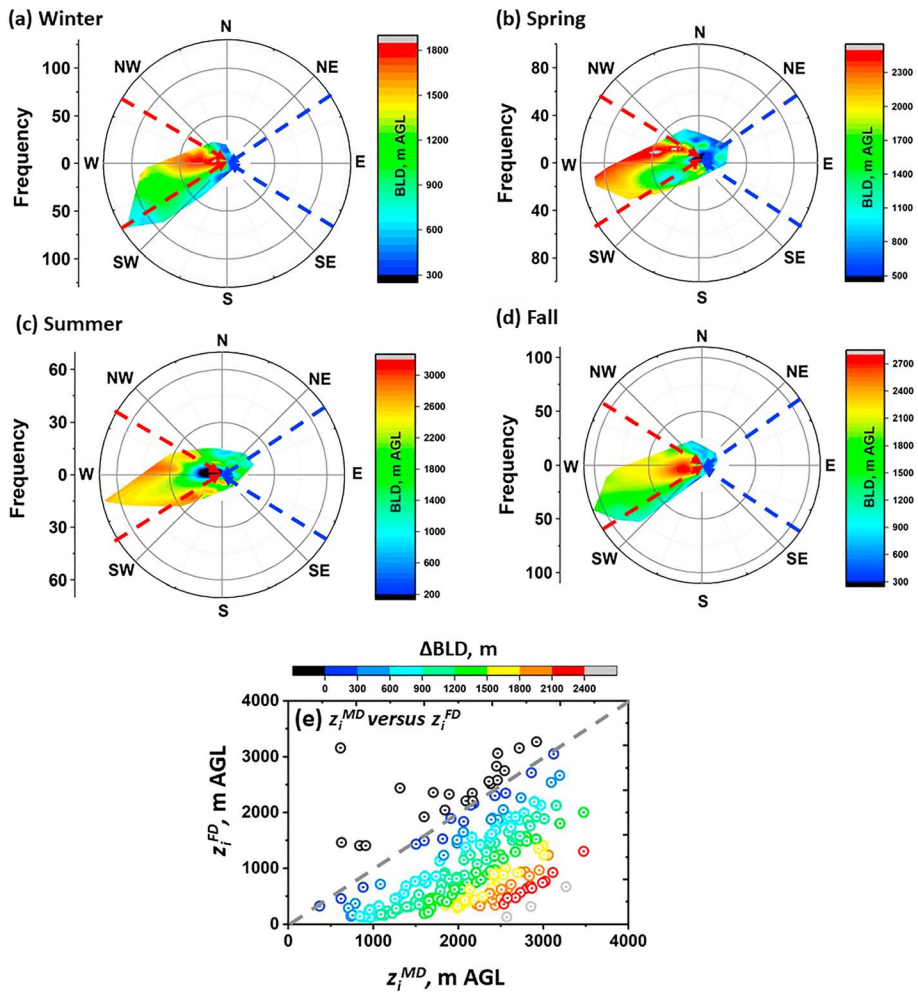

Figure 3. (a) Wind-rose depiction of daily BLDs (color-filled contours) via frequency distribution analysis (BL-WD bin width of 5°) for a 25-year period for the R1 site Great Falls during (a) winter, (b) spring, (c) summer, and (d) fall. Radii denote the frequencies, and angles mark the BL-WD. Red and blue arrows mark the domains of mountain-advected and flatland-advected flows, respectively. (e) Scatterplot of monthly median z_i^{MD} versus z_i^{FD} colored by corresponding ΔBLDs (m) for the entire observation-period (i.e., 300 samples for 25-year period). Dashed gray line marks 1:1 line. BLD = boundary layer depth.

Additionally, both z_i^{MD} and z_i^{FD} yielded typical seasonal-cycle BLD feature over the land surface, as confirmed with their seasonal-cycle BLD amplitudes (seasonal-scale maximum minus minimum BLD, typically observed during summer or spring and winter, respectively). We found BLD amplitudes to be positive for all the R sites though with extreme site-to-site variability: 400–1,500 m and 500–1,600 m for z_i^{MD} and z_i^{FD}, respectively (Figure 4c). High BLD amplitudes over the R sites, particularly over Midland, Del Rio, Santa Teresa, and Riverton, mainly occur due to large seasonal contrasts in surface forcing including large surface-temperature differences between warm and cold seasons, which is a typical meteorological characteristic of arid regions.

On the other hand, the BLD amplitudes for the A sites are not very different from each other and ranges from 500 to 800 m, which could be attributed to (1) low-elevation terrains over the Appalachians compared to the Rockies, (2) relatively smaller contrasts in temperature and surface forcing over the A sites than over the R sites located in warm-temperate-humid climatic regions, and (3) contrasts in meteorological conditions in warm and cold seasons impact on both z_i^{MD} and z_i^{FD} similarly.

We also note that very deep z_i^{MD} (>3,000 m AGL) in spring and summer (Figure 4a) over the three sites (R5-Midland, R5-Santa Teresa, and R5-Del Rio) located in the downstream of central and northwestern portions

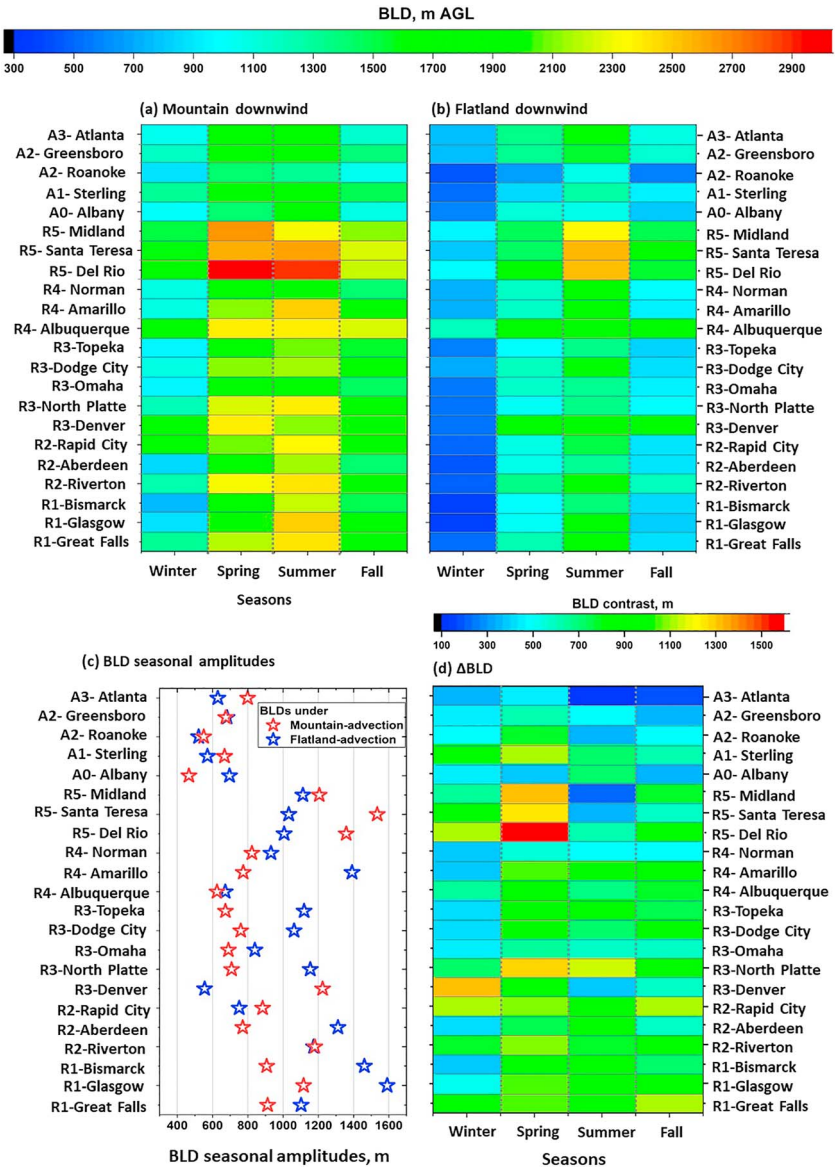

Figure 4. Hovmöller-type diagram of the climatological-average seasonal-cycle patterns of median (a) z_i^{MD}, (b) z_i^{FD}, and (d) relevant ΔBLDs for 22 Integrated Global Radiosonde Archive sites (marked on the *y* axis). Color-bar scale limit (300–2,700 m AGL) for panels a and b kept identical for comparison. (c) Seasonal-scale BLD amplitudes for z_i^{MD} (red star) and z_i^{FD} (blue star). BLD = boundary layer depth.

of the Mexican plateau (Figure 1), which can be attributed to the horizontal advection of EMLs from the plateau. These results also confirm that BLDs over these downwind sites substantially increases as deeper z_i^{MD} advects over the region. Previously, a number of studies (Carlson & Ludlam, 1968; Lanicci & Warner, 1991) found the elevated terrains of Mexico to be one of the major sources of EMLs; these potentially warm EMLs also were found to have a northward expansion into the Rocky Mountains. Figure 4b suggests relatively deeper z_i^{FD} (>2,500 m AGL) over the R5 sites (Midland, Santa Teresa, and Del Rio) compared to the other sites in the Southern Great Plains, which could be attributed to the ABL features over dry warm arid regions like the southwest United States (Lee & Pal, 2017).

Over the sites in central and northern portions of Plains (R3-North Platte, R3-Denver, R2-Rapid City, R2-Riverton, R1-Glasgow, and R1-Great Falls), the observed z_i^{MD} exceeded 2,500 m AGL and were deeper compared to the other sites located along almost similar latitudinal belts (R4-Norman, R3-Topka, R3-Omaha,

R2-Aberdeen, and R1-Bismarck) where z_i^{MD} was around 2,000 m AGL, which could be attributed to the larger distance from the elevated terrains. For instance, Norman, Omaha, and Bismarck are located >750 km east of the source of EMLs (i.e., elevated terrains). Thus, these results indicate that the impact of EMLs is still present miles away from the source, though the strength decreases with distance.

However, one needs greater spatial coverage and much higher spatially resolved information of BLD variability to deduce any analytical relationship about the impact of EMLs as a function of distance. Results reported here are limited in potential in this regard; however, our results on ΔBLDs provide a future pathway to quantify the change of impact of EML with distance. Potential airborne lidar-based investigations in the future would be ideal to explore this relationship, as was shown in Pal et al. (2016), though we note their study was around an isolated mountain. Also, results presented here in this work are of great use for exploring further details of model observation intercomparison studies, for example, as presented in Lee and De Wekker (2016).

Results also reveal significantly shallower z_i^{MD} over the A than over the R sites, particularly in spring and summer; z_i^{FD} did not show such differences between A and R sites (Figure 4). A noteworthy feature in z_i^{MD} and z_i^{FD} is that the impact of elevated terrains on BLDs was not substantial over A3-Atlanta in Georgia because the southern portion of the Appalachians (100 km west of the site) is not very complex with ridges lower than 400 m MSL, whereas the elevation of the rawinsonde site is ~230 m MSL.

3.3. Seasonal-Scale BLD Contrasts Under Mountain Advection Versus Flatland Advection

The climatological-mean seasonal cycles of ΔBLD (seasonal-median z_i^{MD} minus z_i^{FD}) shows strong dependencies on the advection of two different air masses via mountain-advected versus flatland-advected flows (Figure 4d). First, the signs of ΔBLD were found to be positive (100–1,500 m), confirming $z_i^{MD}>z_i^{FD}$ for all sites in all seasons, which appears to be primarily caused by the impact of EMLs on the BLDs over downwind sites of mountains. There exists stronger ΔBLD variability (both spatially and seasonally) among the sites downwind of the Rockies (700–2,700 m) than over the sites located downwind of the Appalachians (300–800 m), which may be potentially attributed to (1) more dominant impacts of EMLs and (2) stronger land-surface forcing due to larger aridity over Rockies than over the Appalachians. Nevertheless, the results presented here provide first-of-a-kind empirical analyses of the ΔBLD seasonal cycles over plains located in the mountains' downstream, thereby reinforcing the concept of BLD footprint under z_i advection off the elevated terrains and its impact miles away from EML sources.

Willis and Deardorff (1976) provided the concept of z_i advection; results presented here provide the empirical evidence on the seasonal-scale changes in ΔBLDs over multiple sites under the influence of z_i advection. Our results primarily demonstrate the "footprint" concept of ABL dynamics under the impact of flows from mountains since both elevated terrains and increased ABL moisture regime over the plains compared to the source regions of EMLs (adiabatic drying of air masses advected off the mountains) contribute to keeping z_i^{FD} below the plateau heights and ridgeline. This favors the formation of EMLs, and thus, z_i^{MD} was deeper than z_i^{FD} in all seasons, particularly in summer and spring.

4. Concluding Remarks

We introduced a "footprint" concept where we represent ABL features over the flat terrains located in mountains' downstream as a function of advected ABL air mass, terrain features, and wind regimes. We computed the daily afternoon BLDs from the 00 UTC soundings using an improved version of the R_{ib} approach, which reduces uncertainties related to shallow BLDs via removing near-surface stable layers (Pal & Lee, 2019). Using a unique classification based on rawinsonde-measured ABL horizontal wind regime, we classified observed BLDs into two types: BLD under mountain advection (z_i^{MD}) and flatland advection (z_i^{FD}). Results reveal that in the presence of orographically induced flows modulating advected-ABL air mass reservoirs in the downwind of mountains, the BLDs over the plains are influenced by the EMLs. Both z_i^{MD} and z_i^{FD} variability revealed typical BLD seasonal cycle patterns over land though with extreme site-to-site variability in seasonal-scale BLD amplitudes (800–1,600 m).

We found that the pattern and magnitude of BLD contrasts under two flow regimes (i.e. ΔBLDs) vary substantially over time (daily, monthly, and seasonal basis), across space (e.g., different distances from

elevated terrains; regions, here R1, R2, etc.; and wind regimes), and variable moisture regimes. For instance, the BLD contrasts were higher downwind of the Rockies than the Appalachians, and higher BLD contrasts were observed in spring and summer (900–1,500 m) than in fall and winter (100–500 m). Results related to the changes in the ΔBLDs with distance from the terrains suffer due to the brevity of observations (intra-site distance of more than 100 km). Furthermore, our findings indicate that ΔBLD dampens with distance; however, more comprehensive high-resolved data sets are needed to confirm this (e.g., frequent rawinsonde launches and dense lidar networks). Nevertheless, our results may serve as an appropriate test bed for the numerical modeling of the impact of advected z_i off elevated terrains on plains.

Overall, our results underscore the importance of advection on ABL thermodynamic features, in particular BLDs over extended regions located in the mountains' downstream. Our results will help build advanced parameterization schemes to improve numerical weather prediction of convection initiation processes over and near mountainous regions where accurate simulations of ABL depths in the mountains' downstream still remains a hurdle. Our analyses will also provide observational constrains for validating numerical models and to improve boundary layer parameterizations so that the observed ΔBLDs could be simulated accurately during four seasons, in particular during the spring and summer.

Acknowledgments
The IGRA rawinsonde data sets were downloaded from ftp://ftp.ncdc.noaa.gov/, and the surface elevation data from the PRISM (Parameter-elevation Regressions on Independent Slopes Model). This work was sponsored by an internal start-up research grant at Texas Tech University, Lubbock, Texas. The results and conclusions, and any views expressed herein, are those of the authors and do not necessarily reflect those of NOAA or the Department of Commerce. Finally, we thank two anonymous reviewers for their constructive criticisms and helpful suggestions.

References

Angevine, W. M., Tjernstrom, M., & Zagar, M. (2006). Modeling of the coastal boundary layer and pollutant transport in New England. *Journal of Applied Meteorology and Climatology*, *45*(1), 137–154. https://doi.org/10.1175/JAM2333.1

Behrendt, A., Pal, S., Aoshima, F., Bender, M., Blyth, A., Corsmeier, U., et al. (2011). Observation of convection initiation processes with a suite of state-of-the-art research instruments during COPS IOP8b. *Quarterly Journal of Royal Meteorological Society*, *137*(S1), 81–100. https://doi.org/10.1002/qj.758

Berman, S., Ku, J. -Y., & Rao, S.-T. (1999). Spatial and temporal variation in the mixing depth over the northeastern United States during the summer of 1995. *Journal of Applied Meteorology*, *38*, 1661–1673. https://doi.org/10.1175/1520-0450(1999)038%3C1661:SATVIT%3E2.0.CO;2

Boutle, I. A., Beare, R. J., Belcher, S. E., Brown, A. R., & Plant, R. S. (2010). The moist boundary layer under a mid-latitude weather system. *Boundary Layer Meteorology*, *134*(3), 367–386. https://doi.org/10.1007/s10546-009-9452-9

Cai, X., Huo, Q., Kang, L., & Song, Y. (2014). Equilibrium atmospheric boundary-layer flow: Computational fluid dynamics simulation with balanced forces. *Boundary-Layer Meteorology*, *152*(3), 349–366. https://doi.org/10.1007/s1054

Carlson, T. N., & Ludlam, F. H. (1968). Conditions for the formation of severe local storms. *Tellus*, *20*(2), 203–226. https://doi.org/10.1111/j.2153-3490.1968.tb00364.x

Davy, R., & Esau, I. (2016). Differences in the efficacy of climate forcings explained by variations in atmospheric boundary layer depth. *Nature Communications*, *7*(1), 2016. https://doi.org/10.1038/ncomms11690

Demko, J. C., Geerts, B., Miao, Q., & Zehnder, J. (2009). Boundary-layer energy transport and cumulus development over a heated mountain: An observational study. *Monthly Weather Review*, *137*(1), 447–468. https://doi.org/10.1175/2008MWR2467.1

Durre, I., Vose, R., & Wuertz, D. (2006). Overview of the integrated global radiosonde archive. *Journal of Climate*, *19*(1), 53–68. https://doi.org/10.1175/JCLI3594.1

Fast, J. D., Doran, J. C., Shaw, W. J., Coulter, R. L., & Martin, T. J. (2000). The evolution of the boundary layer and its effect on air chemistry in the Phoenix area. *Journal of Geophysical Research*, *105*(D18), 22,833–22,848. https://doi.org/10.1029/2000JD900289

Fernando, H. J. S., Pardyjak, E. R., di Sabatino, S., Chow, F. K., de Wekker, S. F. J., Hoch, S. W., et al. (2015). The MATERHORN: Unraveling the Intricacies of Mountain Weather. *Bulletin of American Meteorological Society*, *96*(11), 1945–1967. https://doi.org/10.1175/BAMS-D-13-00131.1

Groenemeijer, P., Barthlott, C., Corsmeier, U., Handwerker, J., Kohler, M., Kottmeier, C., et al. (2009). Observations of kinematics and thermodynamic structure surrounding a convective storm cluster over a low mountain range. *Monthly Weather Review*, *137*(2), 585–602. https://doi.org/10.1175/2008MWR2562.1

Gryning, S.-E., & Batchvarova, E. (1999). Regional heat flux over the NOPEX area estimated from the evolution of the mixed-layer. *Agricultural and Forest Meteorology*, *98-99*, 159–167. https://doi.org/10.1016/S0168-1923(99)00095-7

Guo, J., Li, Y., Cohen, J. B., Li, J., Chen, D., Xu, H., et al. (2019). Shift in the temporal trend in boundary layer height trend in China using long-term (1979–2016) radiosonde data. *Geophysical Research Letters*. https://doi.org/10.1029/2019GL082666

Koffi, E. N., Bergamaschi, P., Karstens, U., Krol, M., Segers, A., Schmidt, M., et al. (2016). Evaluation of the boundary layer dynamics of the TM5 model over Europe. *Geoscientific Model Development*, *9*(9), 3137–3160. https://doi.org/10.5194/gmd-9-3137-2016

Kossmann, M., Vögtlin, R., Corsmeier, U., Vogel, B., Fiedler, F., Binder, H. J., et al. (1998). Aspects of the convective boundary layer structure over complex terrain. *Atmospheric Environment*, *32*(7), 1323–1348. https://doi.org/10.1016/S1352-2310(97)00271-9

Lanicci, J. M., & Warner, T. T. (1991). A synoptic climatology of the elevated mixed-layer inversion over the southern Great Plains in spring. Part I: Structure, dynamics, and seasonal evolution. *Weather Forecasting*, *6*, 181–197. https://doi.org/10.1175/1520-0434(1991)006,0181:ASCOTE.2.0.CO;2

Lee, T. R., & De Wekker, S. F. J. (2016). Estimating daytime planetary boundary layer heights over a valley from rawinsonde observations at a nearby airport: An application to the Page Valley in Virginia, USA. *Journal of Applied Meteorology and Climatology*, *55*(3), 791–809. https://doi.org/10.1175/JAMC-D-15-0300.1

Lee, T. R., De Wekker, S. F. J., & Pal, S. (2018). The impact of the afternoon planetary boundary-layer height on the diurnal cycle of CO and mixing ratios at a low-altitude mountaintop. *Boundary-Layer Meteorology*, *168*(1), 81–102. https://doi.org/10.1007/s10546-018-0343-9

Lee, T. R., & Pal, S. (2017). On the potential of 25 years (1991–2015) of rawinsonde measurements for elucidating climatological and spatiotemporal patterns of afternoon boundary layer depths over the contiguous US. *Advances in Meteorology*, *2017*, 1–19. https://doi.org/10.1155/2017/6841239

Moeng, C. H., & Rotunno, R. (1990). Vertical-velocity skewness in the buoyancy-driven boundary layer. *Journal of the Atmospheric Sciences*, *47*(9), 1149–1162. https://doi.org/10.1175/1520-0469(1990)047<1149:VVSITB>2.0.CO;2

Nyeki, S., Kalberer, M., Colbeck, I., de Wekker, S., Furger, M., Gäggeler, H. W., et al. (2000). Convective boundary layer evolution to 4 km ASL over high-alpine terrain: Airborne lidar observations in the Alps. *Geophysical Research Letters*, *27*(5), 689–692. https://doi.org/10.1029/1999GL010928

Osborne, S. R., Johnson, D. W., Wood, R., Bandy, B. J., Andreae, M. O., O'Dowd, C. D., et al. (2000). Evolution of the aerosol, cloud and boundary-layer dynamic and thermodynamic characteristics during the 2nd Lagrangian experiment of ACE-2. *Tellus*, *52*(2), 375–400. https://doi.org/10.1034/j.1600-0889.2000.00051.x

Pal, S., De Wekker, S. F. J., & Emmitt, G. D. (2016). Investigation of the spatial variability of the convective boundary layer heights over an Isolated Mountain: Cases from the MATERHORN-2012 experiment. *Journal of Applied Meteorology and Climatology*, *55*(9), 1927–1952. https://doi.org/10.1175/JAMC-D-15-0277.1

Pal, S., & Haeffelin, M. (2015). Forcing mechanisms governing diurnal, seasonal, and inter-annual variability in the boundary layer depths: Five years of continuous lidar observations over a suburban site near Paris. *Journal of Geophysical Research: Atmospheres*, *120*, 11,936–11,956. https://doi.org/10.1002/2015JD023268

Pal, S., & Lee, T. R. (2019). Contrasting air mass advection explains significant differences in boundary layer depth seasonal cycles under onshore versus offshore flows. *Geophysical Research Letters*, *46*, 2846–2853. https://doi.org/10.1029/2018GL081699

Pal, S., Xueref-Remy, I., Ammoura, L., Chazette, P., Gibert, F., Royer, P., et al. (2012). Spatiotemporal variability of the atmospheric boundary layer depth over the Paris agglomeration: An assessment of the impact of the urban heat island intensity. *Atmospheric Environment*, *63*, 261–275. https://doi.org/10.1016/j.atmosenv.2012.09.046

Reen, B. P., Stauffer, D. R., Davis, K. J., & Desai, A. R. (2006). A case study on the effects of heterogeneous soil moisture on mesoscale boundary-layer structure in the Southern Great Plains, U.S.A. Part II: Mesoscale modelling. *Boundary-Layer Meteorology*, *120*(2), 275–314. https://doi.org/10.1007/s10546-006-9056-6

Rotach, M. W., & Zardi, D. (2007). On the boundary layer structure over highly complex terrain: Key findings from MAP. *Quarterly Journal of Royal Meteorological Society*, *133*(625), 937–948. https://doi.org/10.1002/qj.71

Seidel, D. J., Ao, C. O., & Li, K. (2010). Estimating climatological planetary boundary layer heights from radiosonde observations: Comparison of methods and uncertainty analysis. *Journal of Geophysical Research*, *115*, D16113. https://doi.org/10.1029/2009JD013680

Seidel, D. J., Zhang, Y., Beljaars, A., Golaz, J. -C., Jacobson, A. R., & Medeiros, B. (2012). Climatology of the planetary boundary layer over the continental United States and Europe. *Journal of Geophysical Research*, *117*, D17106. https://doi.org/10.1029/2012JD018143

Stensrud, D. J. (1993). Elevated residual layers and their influence on surface boundary layer evolution. *Journal of Atmospheric Sciences*, *50*(14), 2284–2293. https://doi.org/10.1175/1520-0469(1993)050<2284:ERLATI>2.0.CO;2

Stull, R. B. (1988). *An introduction to boundary layer meteorology* (p. 666). Dordrecht, Netherlands: Kluwer Academic Publishers. https://doi.org/10.1007/978-94-009-3027-8

Trentmann, J., Keil, C., Salzmann, M., Barthlott, C., Bauer, H. S., Schwitalla, T., et al. (2009). Multi-model simulations of a convective situation in low-mountain terrain in central Europe. *Meteorology and Atmospheric Physics*, *103*(1-4), 95–103. https://doi.org/10.1007/s00703-008-0323-6

Trier, S. B., Chen, F., & Manning, K. W. (2004). A Study of convection initiation in a mesoscale model using high-resolution land surface initial conditions. *Monthly Weather Review*, *132*(12), 2954–2976. https://doi.org/10.1175/MWR2839.1

Vogelezang, D. H. P., & Holtslag, A. A. M. (1996). Evaluation and model impacts of alternative boundary-layer height formulations. *Boundary Layer Meteorology*, *81*(3-4), 245–269. https://doi.org/10.1007/BF02430331

Whiteman, C. D. (2000). *Mountain meteorology: Fundamentals and applications* (p. 355). Oxford University Press; 2000.

Willis, G. E., & Deardorff, J. W. (1976). On the use of Taylor's translation hypothesis for diffusion in the mixed layer. *Quarterly Journal of the Royal Meteorological Society*, *102*(434), 817–822. https://doi.org/10.1002/qj.49710243411

Xie, B., Hunt, J. C. R., Carruthers, D. J., Fung, J. C. H., & Barlow, J. F. (2013). Structure of the planetary boundary layer over Southeast England: Modeling and measurements. *Journal of Geophysical Research: Atmospheres*, *118*, 7799–7818. https://doi.org/10.1002/jgrd.50621